Synergistic effects of micro/nano modifications on electrodes for microfluidic electrochemical ELISA

著者別名	鈴木 博章, 福田 淳二
journal or publication title	Sensors and actuators. B, Chemical
volume	156
number	2
page range	637-644
year	2011-08
権利	(C) 2011 Elsevier B.V. NOTICE: this is the author's version of a work that was accepted for publication in Sensors and actuators. B, Chemical. Changes resulting from the publishing process, such as peer review, editing, corrections, structural formatting, and other quality control mechanisms may not be reflected in this document. Changes may have been made to this work since it was submitted for publication. A definitive version was subsequently published in PUBLICATION, 156, 2, 2011 DOI:10.1016/j.snb.2011.02.010
URL	http://hdl.handle.net/2241/113614

doi: 10.1016/j.snb.2011.02.010

Synergistic effects of micro/nano modifications on electrodes for microfluidic electrochemical ELISA

Sonthaya Numthuam[a], Takahiro Kakegawa[a], Takahisa Anada[b], Ali Khademhosseini[c,d], Hiroaki Suzuki[a], Junji Fukuda[a]*

[a] *Graduate School of Pure and Applied Sciences, University of Tsukuba, Tsukuba, Ibaraki 305-8573, Japan*

[b] *Graduate School of Dentistry, Tohoku University, Sendai, Miyagi 980-8575, Japan*

[c] *Department of Medicine, Brigham and Women's Hospital, Harvard Medical School, Cambridge, MA 02139, USA*

[d] *Harvard-MIT Division of Health Sciences and Technology, Massachusetts Institute of Technology, Cambridge, MA 02139, USA*

* Corresponding author: Tel.: +81-29-853-4995; fax: +81-29-853-4490; E-mail address: fukuda@ims.tsukuba.ac.jp

Abstract

Microfluidic electrochemical sensing has been considered to be highly efficient. In this study, we showed, by using numerical simulations, that a planar electrode formed on the bottom of a microchannel is exposed to only a small fraction of analytes in amperometric detection. We also showed that three-dimensional (3D) micropillar electrodes significantly improve the detection current. The practical performance was evaluated using 3D micropillar electrodes fabricated by photolithography. The output current increased as the diameters of the micropillars decreased, as predicted by the simulations. It is noteworthy that the current enhancements obtained with the 3D electrodes were larger than those expected from an increase in the surface area. Further increase in current was achieved by electrical deposition of nanoporous gold-black onto the surface of the 3D electrode: when a 3D electrode with micropillars 30 μm in diameter was used, the output current was approximately 20 times that obtained with a 2D electrode without modification. The applicability of the micropillar electrodes was demonstrated in electrochemical enzyme-linked immunosorbent assay (ELISA) of bone metabolic marker proteins. Although an increase in the surface area of the electrode leads to more noise in general, there is no significant difference in the signal-to-noise ratio between the modified 3D electrode and the 2D electrode without modification in

the ELISA experiments. This nanoporous micropillar electrode could potentially be a useful component for the development of on-site diagnosis systems.

Keywords: Micropillar electrode; Nanoporous structure; Gold-black; Electrochemical ELISA; Osteoporosis

1. Introduction

There has been a great deal of interest in the miniaturization of analytical systems for bio/chemical sensing applications, which has led to the development of devices commonly known as a micro total analysis system or a lab-on-a-chip [1, 2]. Miniaturized systems offer many potential advantages over conventional assay platforms, including small sample volumes, low cost, short assay time, high throughput, and automation [3, 4]. Systems with integrated electrochemical sensors, in particular, could provide new opportunities in bedside diagnosis and assays for use at home, because of their simplicity and ability to function without expensive equipment [5]. Electrochemical sensors have already been exploited in several diagnostic products, including portable systems for self-monitoring of blood glucose in diabetic patients [6]. Despite such favorable characteristics, a critical issue that arises from the miniaturization of such systems is that they must use a relatively low amount of detection current, which sometimes necessitates the use of laboratory-grade detection instruments for performing reliable measurements.

Electrodes in a typical miniaturized system have a two-dimensional (2D) planar form and are often directly patterned inside a microchannel [7]. Although electrochemical sensing in a microchannel has generally been considered to be highly

efficient, a large proportion of analyte molecules pass over the electrode even in a microchannel [8]. Therefore, most of the analyte does not come into contact with the electrodes and is wasted. This implies that the detection current can be increased by increasing the collection efficiency, which may lead to high sensitivity.

Many nanotechnology-based approaches have been attempted to improve the detection sensitivity. These include modifications of the surface of an electrode with platinum black [9], carbon nanotubes [10], zinc oxide nanorods [11], and other nanostructures [12, 13]. These modifications increase the surface area of the electrode and, in some cases, provide efficient electron transfer, such as in enzymatic sensors. The detection sensitivity is often defined as the signal-to-noise (s/n) ratio, in which the detection current represents the signal and the corresponding standard deviation represents the noise. In general, greater the electrode surface, greater is the noise. Therefore, to improve sensitivity and reduce noise, the use of a microelectrode or nanoelectrode array has been proposed [9, 14]. The effects of the geometry of the microelectrode or nanoelectrode on the detection sensitivity have been systematically investigated. Although some sophisticated sensing systems have been proposed, modifications have mostly been made to the 2D planar electrodes; therefore, the modifications themselves have not necessarily resulted in the collection of a greater

proportion of the analyte molecules that pass over the electrode.

Although microfabrication technologies have been widely used in analytical chemistry, there are only a few studies on an electrode that has 3D microstructures for microfluidic analysis; moreover, no electrodes with 3D microstructures have been developed for the enzyme-linked immunosorbent assay (ELISA). In one such study, an array of micropillar electrodes that were 20 μm in height and 20 μm in diameter were used to eliminate electroactive interferents such as L-ascorbic acid upstream of the detection electrode in the microchannel [15]. In addition, square pillars (~18 μm in height and 20 μm in width) were placed at the end of an electrophoresis microchannel for complete preconcentration and removal of interference in neurotransmitter detection [16]. These studies have clearly demonstrated the efficacy of 3D electrodes in microfluidic bioanalysis.

In this paper, we emphasize the practical applicability of 3D micropillar electrodes further modified with nanoporous structures by electroplating. The efficacy of these 3D electrodes in ELISA is discussed. Micro/nano modifications of electrodes could potentially provide a versatile and fundamental component for the development of portable diagnostic systems with broad applicability.

2. Experimental

2.1. Reagents and materials

Materials used for the fabrication of the 3D micropillar electrodes were obtained from the following commercial sources: Glass wafers (#7740, 3 inch, 500-μm thick), from Corning Japan (Tokyo, Japan); thick film photoresist (SU-8), from Microchem (MA, USA); dry-film photoresist (ME-1048 EA), from Hitachi Chemical Company (Tokyo, Japan); polyimide precursor solution (SP-341), from Toray Industries (Tokyo, Japan); and poly(dimethylsiloxane) (PDMS, KE-1300T), from Shin-Etsu Chemical (Tokyo, Japan).

Reagents used for the characterization of the 3D micropillar electrodes were obtained from the following commercial sources: Human bone alkaline phosphatase (BAP), monoclonal sheep antibodies against human BAP for primary antibody, and biotinylated polyclonal sheep antibody against human BAP for secondary antibodies, from Abcam (MA, USA); human tartrate-resistant acid phosphatase-5b (TRACP-5b), polyclonal antibodies against human TRACP-5b, and biotinylated polyclonal sheep antibodies against human TRACP-5b for secondary antibody, from Abcam (MA, USA); β-galactosidase-streptavidin complex, from Vector Laboratories (Geneva, Switzerland); a blocking solution (Block Ace), from Dainippon Sumitomo Pharmaceutical (Osaka,

Japan); and *p*-aminophenyl-β-D-galactopyranoside, from Sigma-Aldrich (MO, USA). All other reagents were purchased from Wako Pure Chemicals Industries (Tokyo, Japan), unless otherwise noted. Double distilled water was used throughout the experiments.

2.2. Numerical simulation

Numerical simulation was carried out for the device structure shown in Fig. 1A. It was assumed that the three-electrode system was integrated in a microchannel of width 500 μm and height 55 μm. The dimensions and naming convention of the micropillar working electrodes are given in Table 1. The height of the micropillars was 50 μm in all cases, and the diameter and pitch (inter-pillar distance) were set to be equal and homothetic to each other. In the simulation and following experiments, a solution of 1 mM L-ascorbic acid, an electroactive analyte, was passed through the channel at a flow rate of 10 μl/min. The distribution of the flow velocity and concentration in the vicinity of the working electrodes were simulated with the finite difference method using thermo-fluid analysis software (FLOW-3D, Flow Science Inc., Santa Fee, NM, USA). The calculation was carried out on the basis of the following transport-diffusion equation,

$$\frac{\partial C}{\partial t} + \nabla \cdot CU = D\nabla^2 U - D_s AC, \quad \textbf{(1)}$$

where C is the concentration of L-ascorbic acid; U, the flow velocity; D, the diffusion coefficient [here, $D = 1.03 \times 10^{-5}$ cm^2/s [17]]; A, the specific surface area (electrode surface area per partial volume in unit cell); and Ds, the oxidation rate of L-ascorbic acid on the electrode. The value of Ds was estimated by matching the data obtained from calculations and experiments using the planar electrode.

2.3. Fabrication of micropillar electrodes

Micropillar electrodes with dimensions similar to those in the numerical simulation, except for the ø5 μm electrode, were fabricated and their performance was characterized experimentally. The electrodes were fabricated using conventional photolithography techniques including sputter-deposition of metals, photoresist patterning, chemical etching, and lift-off. A gold layer (230 nm) was first deposited on a glass wafer with a chromium intermediate layer (60 nm) and patterned for the working and auxiliary electrodes. The active area of the working electrode was 500 μm × 500 μm. The reference electrode was formed with a silver layer (650 nm). A polyimide layer (3.0 μm) was formed to delineate the active areas for the electrodes and the pad areas. The silver layer was also covered with the polyimide layer, except for two pinholes of 70 μm diameter, which were used to make the reference electrode durable in a

concentrated KCl solution [18]. Subsequently, an array of micropillars was fabricated on the active area of the gold working electrode with a thick film photoresist SU-8. A gold layer (230 nm) was again sputter-deposited on the working electrode with the micropillars through a stainless steel mask with a 500 μm × 500 μm square hole. The wafer was then cut into small pieces (20 mm × 15 mm). Prior to experiments, a silver chloride layer was grown from the pinholes by applying 50 nA for 5 min in a 0.1 M KCl solution with respect to a platinum plate electrode.

The microdevice shown in Fig. 1a comprises a glass substrate patterned with electrodes and a PDMS microchannel. The PDMS microchannel was fabricated with a SU-8 mold by casting liquid prepolymers composed of a mixture of 10:1 silicon elastomer and the curing agent [19]. The mixture was cured at 80°C for 1 h, and the PDMS replica was then peeled off from the mold. The width and height of the microchannel were 500 μm and 55 μm, respectively. Finally, the PDMS substrate was aligned and placed on the substrate with the electrodes under a microscope, and was reversibly sealed by applying slight pressure between the two substrates.

2.4. Modification of the electrode surface with gold-black

The surface of the micropillar electrodes was modified with gold-black. To

optimize the plating current density, gold-black was deposited on the planar electrode under six constant current densities, from –20 to –480 μA/mm^2, for 5 min in a vigorously stirred solution containing 83 mM hydrogen tetrachloroaurate(III) tetrahydrate and 1.58 mM lead(II) acetate [20]. The presence of the gold-black layer on the electrodes was observed using a scanning electron microscope (TM-1000, Hitachi, Tokyo, Japan). The thickness of the gold-black layer was measured using a laser scanning microscope (VK-9700, Keyence, Osaka, Japan). The effect of the modification was examined with L-ascorbic acid, as described below. Based on the results with the planar electrode, the ø30-μm electrode was modified at –60 μA/mm^2.

2.5. Measurement procedures

Planar and micropillar electrodes with or without gold-black were characterized by measuring the oxidation current of L-ascorbic acid in the microdevice, as shown in Fig. 1a, under conditions similar to those used for the numerical simulation. A solution of 1 mM L-ascorbic acid was injected into the microchannel at a flow rate of 10 μl/min by using a microsyringe pump (KdScientific, MA, USA). A potential of +0.7 V with respect to the Ag/AgCl reference electrode was applied to the working electrode by using a potentiostat (HA-151, Hokuto Denko, Tokyo, Japan). On the electrode,

L-ascorbic acid was oxidized to L-dehydroascorbic acid and the converged oxidation current was measured.

2.6. Electrochemical ELISA

The 3D electrode with gold-black was used to detect the two bone metabolic marker proteins, BAP and TRACP-5b, by using the setup shown in Fig. 1b. In this scheme, the reactions required for ELISA were performed upstream, on the surface of PDMS micropillars fabricated in a serpentine channel. The enzymatically converted analytes were then detected downstream with the 3D working electrode. The procedures used to fabricate the PDMS substrate and glass substrate with the electrodes were the same as those mentioned above, whereas the PDMS had a serpentine channel in which PDMS micropillars were formed. The SU-8 master for the PDMS mold was fabricated using a corresponding mask. Prior to the curing of the PDMS prepolymers, air bubbles in the concave wells were removed by placing the assembly in vacuum for at least 30 min. The serpentine channel was 55 μm in height, 500 μm in width, and 50 mm in length. The PDMS micropillars were 55 μm in height and 50 μm in diameter. The inter-pillar distance (edge to edge) was 50 μm. The number of PDMS micropillars was approximately 6000.

The ELISA reactions were carried out on the surface of the PDMS micropillars in the serpentine channel. First, the primary antibody was immobilized on the surface by using a covalent binding method [21]. Briefly, the PDMS substrate was immersed in acetone for 5 m, washed with distilled water, and immersed in 30%(v/v) hydrogen peroxide for 1 h. The surface was then reacted with 2.0%(v/v) 3-aminopropyl-triethoxysilane for 2 h at room temperature and subsequently for 5 min at 50°C. After washing with acetone, the PDMS substrate was placed on a plain glass substrate. The amino group on the PDMS surface was activated by passing 5.0%(v/v) glutaraldehyde at a flow rate of 1 μl/min for 1 h. During this step, the color of PDMS changed to light orange. After washing with distilled water, 20 μg/ml primary antibodies against human BAP or TRACP-5b was introduced into the microchannel at a flow rate of 1 μl/min for 10 min. To inhibit non-specific adsorption of proteins, a blocking solution (Block Ace) was passed for 10 min and the substrate was then washed with PBS.

A series of BAP or TRACP-5b solutions of different concentrations were prepared and introduced into the microchannel at a flow rate of 1 μl/min for 10 min. After washing with PBS, 20 μg/ml secondary biotinylated antibodies against human BAP or TRACP-5b was introduced into the microchannel at a flow rate of 1 μl/min and made to

react with the immobilized bone metabolic marker proteins for 10 min. Then, 0.5 U/ml β-galactosidase-streptavidin complex was introduced at a flow rate of 1 μl/min and allowed to react with the secondary antibodies labeled with biotin for 15 min. The PDMS substrate was subsequently peeled off from the initial glass substrate and placed on the glass substrate with the ø30-μm electrodes with gold-black. Finally, 4.5 μM *p*-aminophenyl-β-D-galactopyranoside, a substrate for β-galactosidase, was introduced into the microchannel at the flow rate of 1 μl/min. The enzyme converts *p*-aminophenyl-β-D-galactopyranoside to *p*-aminophenol. The potential was kept at +0.3 V with respect to the Ag/AgCl reference electrode, and the output current caused by oxidation of *p*-aminophenol to *p*-quinoneimine on the electrode was measured with a potentiostat (Autolab PGSTAT12, Eco Chemie, Utrecht, Netherlands).

3. Results and discussion

3.1. Numerical evaluation of 3D micropillar electrodes

Fluid flow and electrochemical reactions were simulated with the 3D numerical calculation method to investigate the effect of 3D geometry on the increase in the sensitivity of the electrodes. It was assumed that 1 mM L-ascorbic acid solution was introduced into the microchannel and oxidized at the electrode. The distribution of the

analyte concentration clearly showed that only a fraction of the analyte passing in proximity to the 2D planar electrode was consumed, and that most analytes passed over the electrode without any reaction even in the relatively thin microchannel of height 55 µm and width 500 µm (Fig. 2a). We hypothesized that 3D micropillars protruding from the bottom of the microchannel may be beneficial for disturbing the flow stream; moreover, they increase the surface area of the electrodes, thereby improving the detection current. The dimensions of the 3D electrodes used for the simulation are given in Table 1. The ø30-µm electrode did not affect the fluid flow profiles and the concentration distribution significantly; as expected, pillars with smaller diameters had a more significant effect on the concentration distribution (Fig. 2a). As indicated by the extent of the blue region in the outlet of the channels (see Fig. 2a), which has a lower analyte concentration, more analyte was consumed in channels with smaller micropillars. The consumption rate with the ø5-µm electrode was approximately five times higher than that with the planar electrode (Fig. 2b).

The numerical simulation also predicted a critical issue in the fabrication process. A channeling flow was generated at the interspaces between the micropillars and the walls of the microchannel when the micropillars with smaller diameters (ø10 µm and ø5 µm) were used; the ø30-µm electrode caused no significant channeling flow (Fig. 2c). Such

locally concentrated flow may cause excessive pressure and poor reproducibility in the experimental investigation. As described in the Experimental section, the 3D electrode was patterned on a glass substrate and the microchannel was made from PDMS, and these substrates were aligned and bonded under a microscope. Thus, there is a technical limitation to the precision of alignment and the interspaces were set to be over 30 μm even in the ø10-μm and ø5-μm electrodes.

3.2. Experimental evaluation of 3D electrodes

To experimentally measure the effect of the 3D electrodes, electrodes with dimensions the same as those used for the simulation, except the ø5-μm electrode, were fabricated (Figs. 3a–c). The height of the micropillars was 50 ± 2.3 μm; the diameter was 30 ± 1.5 μm for the ø30-μm electrode, 20 ± 2.3 μm for the ø20-μm electrode, and 10 ± 1.8 μm for the ø10-μm electrode. The efficiency of the electrodes was evaluated with L-ascorbic acid under the same conditions as those used in the simulations. As expected, our experiments demonstrated that the oxidation current increased with a decrease in the diameter of the micropillars (Fig. 4, open bar). A 12-fold increase was observed with the ø10-μm electrode compared with the planar electrode, which was considerably greater than that predicted in the simulation (3.5-fold). In addition, the

current enhancements with the 3D electrodes were larger than the current enhancements expected from increases in surface area. For example, in the case of the ø10-µm electrode, a 12-fold increase was observed in current although the increase in surface area was only 4.4-fold. This increase may have been caused by the effects of unsteady-state fluid flow around the micropillars and complicated fluid patterns such as vortex-wake flow. Although detection with the 3D electrode became more effective by miniaturizing the micropillars, fabrication became increasingly more difficult and acquisition of reproducible data was difficult with the ø5-µm electrode (data not shown). As observed from the simulation, channeling flow might also cause poor reproducibility.

3.3. Efficacy of the modification of 3D electrode with gold-black

Gold-black is typically formed by a vapor deposition process, in which colloidal gold particles (~10 nm in diameter) adhere to each other on a substrate to form a nanoporous layer [22]. Although vapor-deposited gold-black is widely used for sensors such as bolometers and thermocouples, the resulting layers are often not stable enough for electrochemical sensing in a solution. There is a large body of literature on the use of vapor-deposited gold-black; studies on electrochemically deposited gold-black, in

contrast, are relatively few [20, 23]. Electrodeposited gold-black and platinum black have been deposited on auxiliary electrodes to reduce the current density [24]. In this study, we investigated whether the efficiency of 3D micropillar electrodes can be increased by electrical modification, that is, by depositing gold-black on the surface of the electrodes; this method could potentially serve as a simple and reproducible method of increasing electrode efficiency. Prior to using the 3D electrode, a planar electrode was used to optimize the electrodeposition conditions with different current densities from −20 to −480 μA/mm^2. The appearance of the deposited gold-black was dependent largely on the current density (Figs. 3c–g). On increasing the current density, the fine structure grew and finally coalesced at current densities of over −120 μA/mm^2 (Fig. 3f). These electrodes were also evaluated with L-ascorbic acid. Compared with the electrode modified at −20 μA/mm^2, the output current increased 1.4 ± 0.3-fold at −40 μA/mm^2 and 1.9 ± 0.4-fold at −60 μA/mm^2, although further increases had no effect; in fact, the output current decreased 1.6 ± 0.3-fold at −120 μA/mm^2 and 1.5 ± 0.4-fold at −240 μA/mm^2. Based on the results, the ø30-μm electrode was modified at –60 μA/mm^2 (Fig. 3h). The thickness of the gold-black layer was approximately 250 nm. A ø30-μm electrode without modification had no significant effect on the output current; after modification, the output current increased considerably, to levels exceeding those of the

ø10 electrode without modification (Fig. 4). The output current was approximately 20 times greater than that with the 2D electrode without modification.

3.4. ELISA using the 3D electrode modified with gold-black

To demonstrate the applicability of the 3D electrode modified with gold-black, we attempted to detect bone metabolic marker proteins BAP and TRACP-5b using electrochemical ELISA. BAP and TRACP-5b are secreted from osteoblasts and osteoclasts, which are responsible for bone formation and resorption, respectively. Because these two types of cells play an important role in the mineralization of the bone matrix *in vivo*, their metabolic markers seem to be more promising for indicating osteogenesis than other typical examinations such as bone densitometry [25, 26].

As a reaction site for antigen-antibody binding, the PDMS micropillars were placed in the upstream region of the serpentine microchannel, and the 3D electrode was positioned downstream (Fig. 2b). After introducing the solutions required for ELISA, enzymatically converted *p*-aminophenol was detected with the ø30-µm electrode modified with gold-black and an unmodified 2D electrode (Fig. 5). In the detections of BAP and TRACP-5b, a linear relationship was observed between the output current and concentration of the proteins in the case of both 2D and 3D electrodes. The detected

concentration range of BAP included the normal level of 7.9–29.0 U/L in the blood [27]. The average TRACP-5b concentration in normal women is 2.83 ± 1.1 U/L, and it increases with age [28]. Therefore, it is important to detect any abnormal increases in TRACP-5b activity at an early stage. Concentrations ranging from the normal level to 20 U/L could be detected using this device (Fig. 5b). Comparisons of the slopes of the plots show approximately 8- and 10-fold increases in the output current in the cases of BAP and TRACP-5b, respectively, when the 3D electrode modified with gold-black was used. The surface area of the 3D electrode without gold-black was only 1.7 times greater than that of the 2D electrode (Table 1). The current density shown in Fig. 5 was calculated with the surface area without gold-black. The relationship between the current densities of 3D and 2D electrodes was almost identical to that for the output currents (Fig. 5). These results suggest that it is not only the mass transfer (convection and diffusion) that limits the detection efficiency but also the reaction processes on the electrode. Meanwhile, the increases in the output current were not as large as expected from the experiments with L-ascorbic (20-fold increase, Fig. 4). This is most likely due to the differences in flow rate, since in the ELISA experiments, the flow rate (1 µl/min) was one-tenth that in the experiments with L-ascorbic acid (10 µl/min). The diffusion layer formed over an electrode in a flowing stream depends on the flow rate. When the

flow rate is decreased, the diffusion layer thickness and the contribution of the 3D electrode reduce. Furthermore, because the ELISA test is complicated, estimating the influence of the flow rates is not necessarily easy. A slower flow rate reduces the supply of enzyme substrates, leading to a decrease in the detection current. On the other hand, a faster flow rate increases the supply of substrates but decreases the output current because the fraction of substrates converted by the enzymatic reaction decreases. Further studies with numerical simulations and experiments are required to obtain the optimal conditions.

A conventional ELISA performed using a multi-well plate and a spectrometer exhibits high reproducibility and sensitivity (e.g., detection limit: 0.7 U/L of BAP, Quidel®, TECOmedical AG, Switzerland); this electrochemical system also demonstrates high performance since it is able to detect marker proteins in the normal ranges in the blood. It is also noteworthy that the reaction time for each antigen-antibody binding could be reduced to 10 min because of the short diffusion distance in the microchannel. On the other hand, an electrode with greater surface leads to more noise in general. Here, the signal-to-noise (s/n) ratio is defined such that the obtained current represents the signal and the corresponding standard deviation represents the noise. Calculations from the data plotted in Fig. 5 indicate that the

average s/n ratios with 2D and 3D electrodes are 11.6 ± 6.0 and 9.0 ± 3.3 in BAP and 12.5 ± 4.7 and 12.1 ± 5.2 in TRACP-5b, respectively. Thus, there is no significant difference in the s/n ratio in the ELISA experiments. The larger output current should be beneficial because it facilitates the use of a portable and cheap electrochemical instrument without specially designed noise reduction circuits.

4. Conclusions

A microfluidic device with 3D micropillar electrodes was developed for bio/chemical analyses. Numerical simulations and experiments revealed that the output current from the oxidation of L-ascorbic acid could be increased by using the 3D electrode, depending on the dimensions of the micropillar structure. The increase in output current experimentally observed with a ø10-μm electrode was 12-fold as compared to that with a 2D planar electrode. However, the ø5-μm electrode could not be used for stable and reproducible acquisition of data probably due to the channeling flow generated at the uncontrollable interspaces between the micropillars and the walls of the microchannel. Gold-black was electrochemically deposited onto the surface of the micropillars. This modification caused a significant increase in the output current. In particular, the output current with the ø30-μm electrode was greater than that with an

unmodified ø10-µm electrode. The efficacy of the 3D electrode was further demonstrated in the electrochemical ELISA of bone metabolic marker proteins. In this study, antigen-antibody reactions were carried out upstream on the PDMS micropillar surface. A more direct approach in which the reactions are performed on the micropillars of the 3D working electrode could lead to a simpler and more efficient analysis system and is an area of active research [29]. This versatile and efficient 3D micropillar electrode could potentially be a fundamental tool for the development of more sophisticated on-site diagnosis systems.

Acknowledgments

This study was supported by the Industrial Technology Grant Program from New Energy and Industrial Technology Development Organization (NEDO) of Japan. This work was performed in Japan. We would like to thank Dr. Hideki Kuramitz and Dr. Ioana Voiculescu for their scientific and technical supports.

References

[1] P.S. Dittrich, K. Tachikawa, A. Manz, Micro total analysis systems. Latest advancements and trends, Anal. Chem. 78 (2006) 3887–3907.

[2] G.M. Whitesides, The origins and the future of microfluidics, Nature 442 (2006) 368–373.

[3] T. Thorsen, S.J. Maerkl, S.R. Quake, Microfluidic large-scale integration, Science 298 (2002) 580–584.

[4] W. Satoh, S. Takahashi, F. Sassa, J. Fukuda, H. Suzuki, On-chip culturing of hepatocytes and monitoring their ammonia metabolism, Lab on a Chip 9 (2009) 35–37.

[5] X.L. Xu, S. Zhang, H. Chen, J.L. Kong, Integration of electrochemistry in micro-total analysis systems for biochemical assays: Recent developments, Talanta 80 (2009) 8–18.

[6] M. Miyashita, N. Ito, S. Ikeda, T. Murayama, K. Oguma, J. Kimura, Development of urine glucose meter based on micro-planer amperometric biosensor and its clinical application for self-monitoring of urine glucose, Biosens. Bioelectron. 24 (2009) 1336–1340.

[7] J. Wang, Electrochemical detection for microscale analytical systems: a review, Talanta 56 (2002) 223–231.

[8] M. Hashimoto, S. Upadhyay, H. Suzuki, Dependence of the response of an amperometric biosensor formed in a micro flow channel on structural and conditional parameters, Biosens. Bioelectron. 21 (2006) 2224–2231.

[9] M. E. Sandison, N. Anicet, A. Glidle and J. M. Cooper, Optimization of the geometry and porosity of microelectrode arrays for sensor design, Anal. Chem. 74 (2002) 5717–5725.

[10] A.G. Crevillen, M. Pumera, M.C. Gonzalez, A. Escarpa, Towards lab-on-a-chip approaches in real analytical domains based on microfluidic chips/electrochemical multi-walled carbon nanotube platforms, Lab on a Chip 9 (2009) 346–353.

[11] X.X. Lu, H.P. Bai, P. He, Y.Y. Cha, G.M. Yang, L. Tan, Y.H. Yang, A reagentless amperometric immunosensor for alpha-1-fetoprotein based on gold nanowires and ZnO nanorods modified electrode, Anal. Chim. Acta. 615 (2008) 158–164.

[12] J. Wang, D.F. Thomas, A. Chen, Nonenzymatic electrochemical glucose sensor based on nanoporous PtPb networks, Anal. Chem. 80 (2008) 997–1004.

[13] J.H. Yuan, K. Wang, X.H. Xia, Highly ordered platinum-nanotubule arrays for amperometric glucose sensing, Adv. Funct. Mater. 15 (2005) 803–809.

[14] M.E. Sandison, J.M. Cooper, Nanofabrication of electrode arrays by electron-beam and nanoimprint lithographies, Lab on a Chip 6 (2006) 1020–1025.

[15] K. Hayashi, R. Kurita, T. Horiuchi, O. Niwa, Microfabricated on-line electrochemical flow cell integrated with small volume pre-reactor for highly selective detection of biomolecules, Electroanalysis 14 (2002) 333–338.

[16] R.S. Pai, K.M. Walsh, M.M. Crain, T.J. Roussel, D.J. Jackson, R.P. Baldwin, R.S. Keynton, J.F. Naber, Fully Integrated Three-Dimensional Electrodes for Electrochemical Detection in Microchips: Fabrication, Characterization, and Applications, Anal. Chem. 81 (2009) 4762–4769.

[17] C.R. Wilke, P. Chang, Correlation of diffusion coefficients in dilute solutions, AIChE J. 1 (1955) 264–270.

[18] H. Suzuki, T. Taura, Thin-Film Ag/AgCl Structure and Operational Modes to Realize Long-Term Storage, J. Electrochem. Soc. 148 (2001) E468–E474.

[19] D.C. Duffy, J.C. McDonald, O.J.A. Schueller, G.M. Whitesides, Rapid prototyping of microfluidic systems in poly(dimethylsiloxane), Anal. Chem. 70 (1998) 4974–4984.

[20] S. Toyama, O. Takei, M. Tsuge, R. Usami, K. Horikoshi, S. Kato, Surface plasmon resonance of electrochemically deposited Au-black, Electrochem. Commun. 4 (2002) 540–544.

[21] W. Limbut, S. Loyprasert, C. Thammakhet, P. Thavarungkul, A. Tuantranont, P. Asawatreratanakul, C. Limsakul, B. Wongkittisuksa, P. Kanatharana, Microfluidic conductimetric bioreactor, Biosens. Bioelectron. 22 (2007) 3064–3071.

[22] W.R. Blevin, W.J. Brown, Black Coatings for Absolute Radiometers, Metrologia 2 (1966) 139–143.

[23] S. Toyama, M. Someya, O. Takei, T. Ohtake, R. Usami, K. Horikoshi, Y. Ikariyama, Fabrication and characterization of gold-platinum black electrode, Chem. Lett. 2 (2001) 160–161.

[24] A.M. Feltham, M. Spiro, Platinized platinum electrodes, Chem. Rev. 71 (1971) 177–193.

[25] P. Bergmann, J.J. Body, S. Boonen, Y. Boutsen, J.P. Devogelaer, S. Goemaere, J.M. Kaufman, J.Y. Reginster, V. Gangji, A.B.B. Markers, Evidence-based guidelines for the use of biochemical markers of bone turnover in the selection and monitoring of bisphosphonate treatment in osteoporosis: a consensus document of the Belgian Bone Club, Int. J. Clin. Pract. 63 (2009) 19–26.

[26] M. Ueda, M. Inaba, S. Okuno, Y. Maeno, E. Ishimura, T. Yamakawa, Y. Nishizawa, Serum BAP as the clinically useful marker for predicting BMD reduction in diabetic hemodialysis patients with low PTH, Life Sci. 77 (2005) 1130–1139.

[27] Y. Nishizawa, T. Nakamura, H. Ohta, K. Kushida, I. Gorai, M. Shiraki, M. Fukunaga, T. Hosoi, T. Miki, O. Chaki, S. Ichimura, K. Nakatsuka, M. Miura, C.G.U.B. Marker, Guidelines for the use of biochemical markers of bone turnover in osteoporosis (2004), J. Bone Miner. Metab. 23 (2005) 97–104.

[28] T.Y. Chao, C.L. Ho, S.H. Lee, M.M.J. Chen, A. Janckila, L.T. Yam,

Tartrate-Resistant Acid Phosphatase 5b as a Serum Marker of Bone Metastasis in Breast Cancer Patients, J. Biomed. Sci. 11 (2004) 511–516.

[29] S. Numthuam, T. Ginoza, M. Zhu, H. Suzuki, J. Fukuda, Gold-black micropillar electrodes for microfluidic ELISA of bone metabolic markers, Analyst, in press.

Figure captions

Figure 1

Schematic of microdevice containing 3D micropillar electrodes and a microchannel. (a) Device used to characterize the 3D electrodes with L-ascorbic acid in numerical simulation and experiments. (b) Device used for electrochemical ELISA. Reactions for ELISA were carried out upstream on the surface of the PDMS micropillars and the enzymatically generated electroactive analytes were detected downstream by the micropillar electrodes. W.E., working electrode (Au); R.E., reference electrode (Ag/AgCl); A.E., auxiliary electrode (Au).

Figure 2

Calculated results of concentration and flow velocity distributions around the 3D micropillar electrodes. (a) Distribution of the concentration of L-ascorbic acid in the central cross section along the microchannel (side view). The solution flows from the left to the right, and L-ascorbic acid is oxidized and consumed at the electrode. Lower concentrations of L-ascorbic acid are shown in blue. (b) Rate of consumption of L-ascorbic acid calculated from the mass balance between the inlet and outlet. (c) Distribution of flow velocity in the horizontal cross section at the middle height of the

microchannel (top view). The magnified views show the flow streams between the micropillars and the lateral walls of the microchannel. The solution flows from the left to the right and is disturbed by the 3D electrode. Higher velocities are shown in red. The microchannel was 500 µm in width and 55 µm in height. The dimensions of the micropillar electrodes are listed in Table 1.

Figure 3. Scanning electron microscopy images of the working electrodes. (a–c) Micropillar electrodes of ø30 µm (a), ø20 µm (b), and ø10 µm (c). The scale bars are 100 µm. (d–g) The surface of the planar electrode modified with gold-black at a current density of –30 µA/mm^2 (d), –60 µA/mm^2 (e), –120 µA/mm^2 (f), and an unmodified planar electrode (g). The scale bars are 2.5 µm. (h–i) Surface of a micropillar of the ø30-µm electrode modified with gold-black at –60 µA/mm^2 (h) and without modification (i). The scale bars are 10 µm.

Figure 4

Effects of dimensions of the micropillar electrodes and the modification with gold-black on oxidation current of L-ascorbic acid. Gray column, with gold-black; white column, without gold-black. The error bars indicate standard deviation (SD) calculated from at

least three independent experiments for each plot.

Figure 5

Detection of BAP and TRACP-5a by electrochemical ELISA. BAP (a) and TRACP-5a (b) were detected by a ø30-µm electrode modified with gold-black (square) and a planar electrode without any modification (circle), respectively. The error bars indicate SD calculated from at least three independent experiments for each plot. Regression analysis was carried out and correlation coefficients and lines were indicated for each electrode condition.

Table 1. Dimensions of 3D micropillar working electrode

	Planar	ø30 μm	ø20 μm	ø10 μm	ø5 μm
Diameter (μm)	-	30	20	10	5
Pitch (μm)*	-	30	20	10	5
Number of pillars	-	36	143	550	2244
Surface area (mm^2)	0.25	0.42	0.70	1.11	2.01
Area ratio**	1.0	1.7	2.8	4.4	8.0

* Distance from surface to surface

** Relative value calculated with respect to the flat electrode

Fig. 1

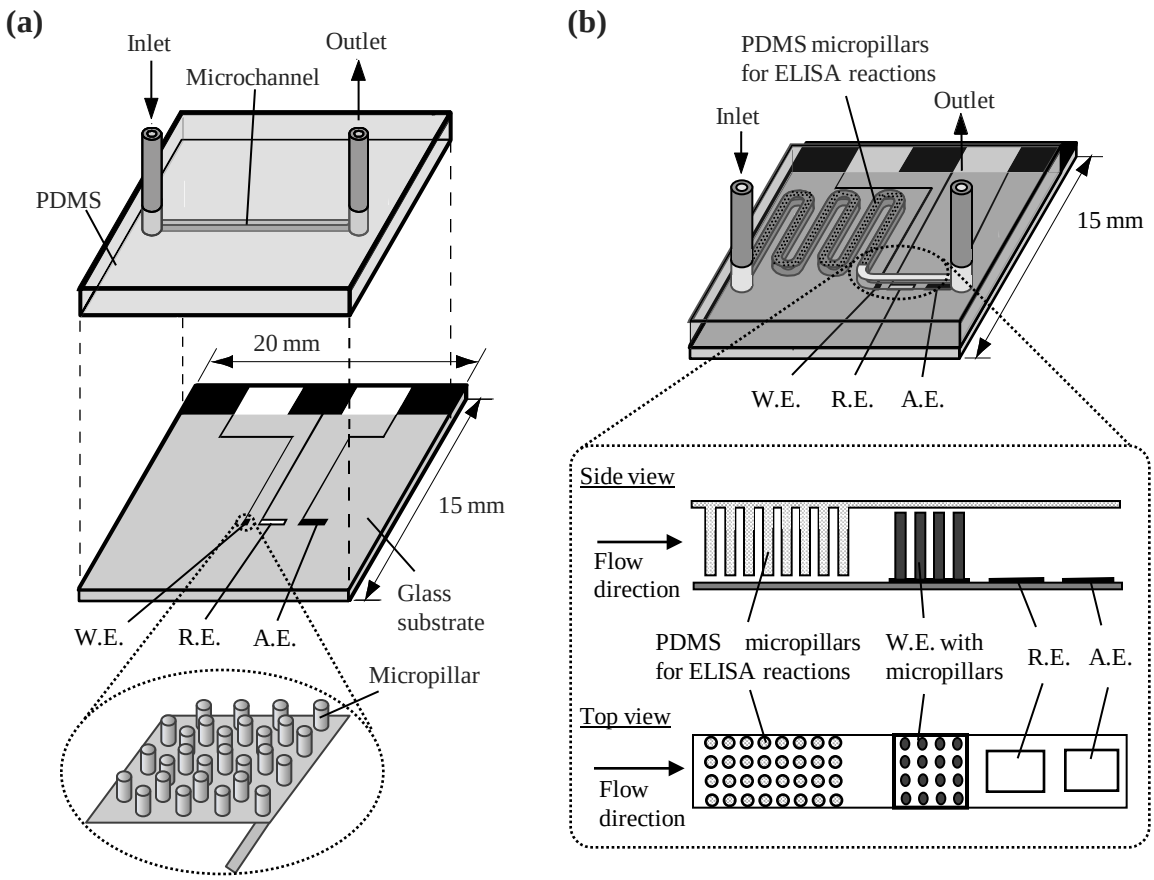
(a)
Inlet
Outlet
Microchannel
PDMS
20 mm
15 mm
Glass substrate
W.E.
R.E.
A.E.
Micropillar
(b)
PDMS micropillars for ELISA reactions
Inlet
Outlet
15 mm
W.E.
R.E.
A.E.
Side view
Flow direction
PDMS micropillars for ELISA reactions
W.E. with micropillars
R.E.
A.E.
Top view
Flow direction

Fig. 2

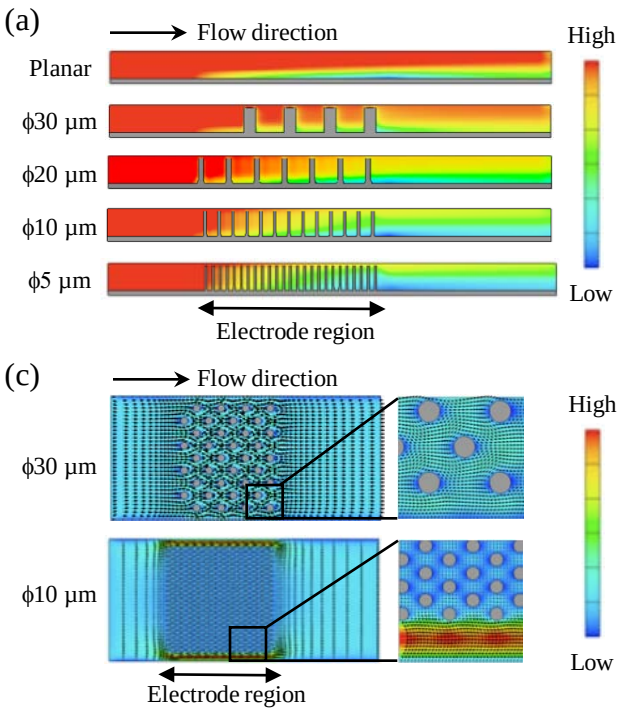
(a)
Flow direction
High
Planar
ϕ30 μm
ϕ20 μm
ϕ10 μm
ϕ5 μm
Low
Electrode region
(c)
Flow direction
High
ϕ30 μm
ϕ10 μm
Low
Electrode region

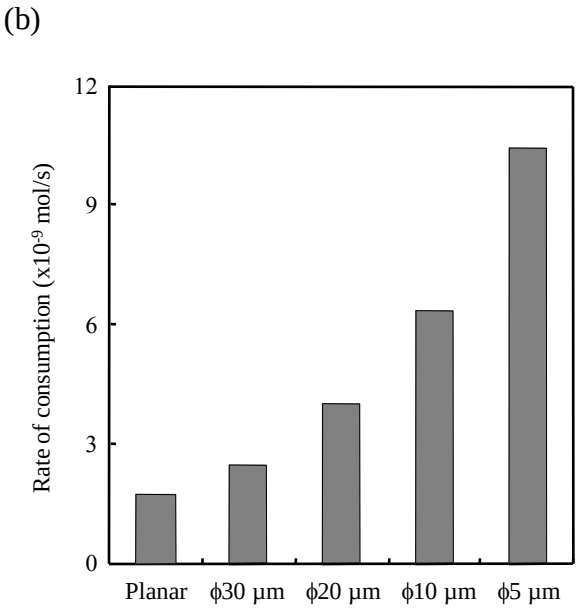
(b)
Rate of consumption (x10-9 mol/s)
12
9
6
3
0
Planar
ϕ30 μm
ϕ20 μm
ϕ10 μm
ϕ5 μm

Fig. 3

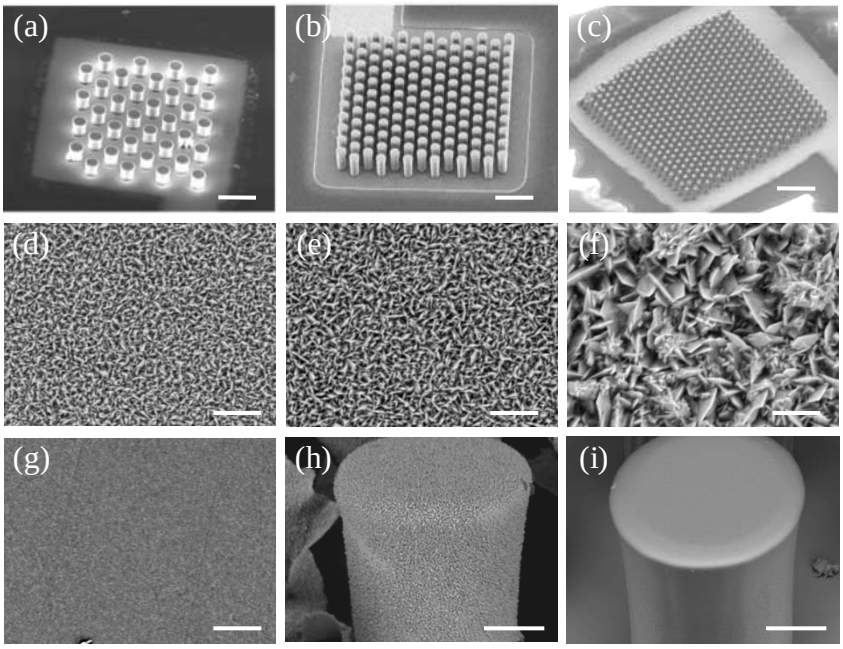

Fig. 4

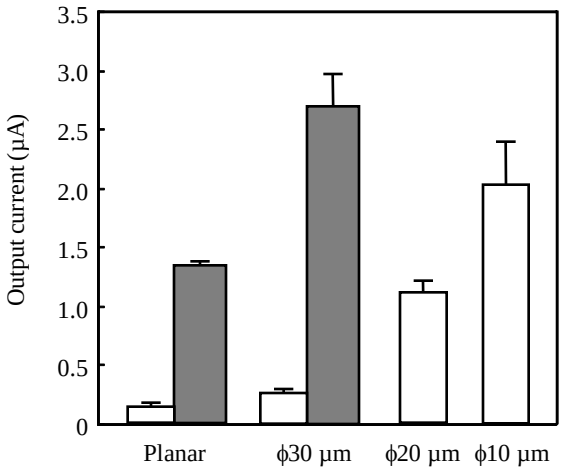
Output current (μA)
3.5
3.0
2.5
2.0
1.5
1.0
0.5
0
Planar
ϕ30 μm
ϕ20 μm
ϕ10 μm

Fig. 5

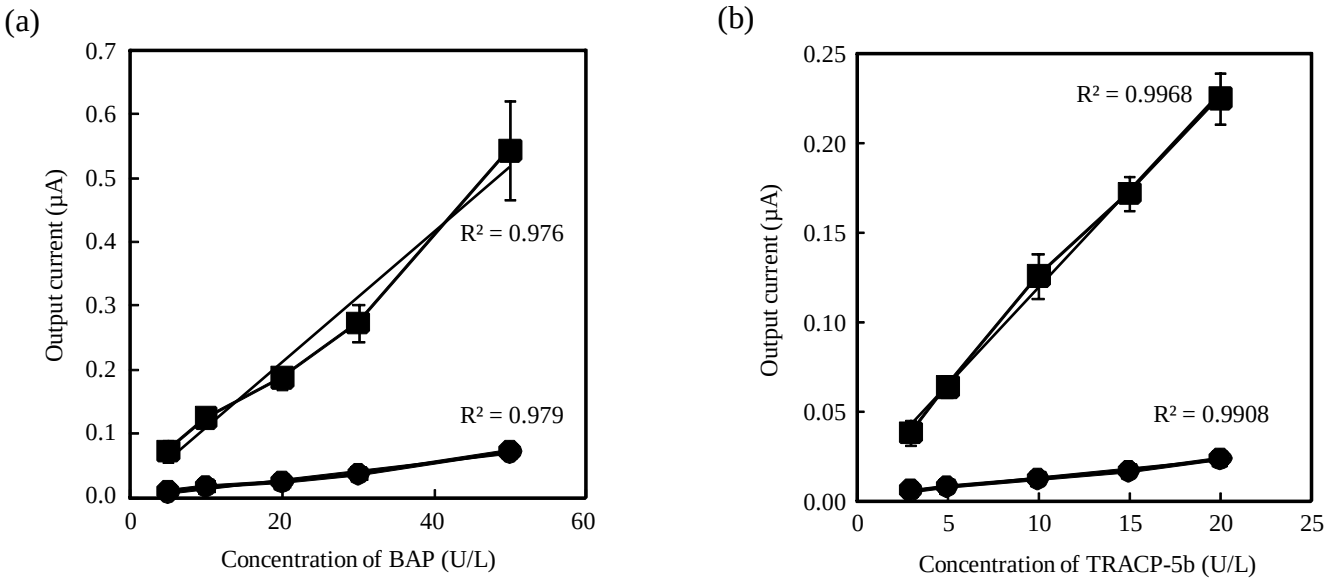
(a)
Output current (μA)
0.7
0.6
0.5
0.4
0.3
0.2
0.1
0.0
0
20
40
60
Concentration of BAP (U/L)
R² = 0.976
R² = 0.979
(b)
Output current (μA)
0.25
0.20
0.15
0.10
0.05
0.00
0
5
10
15
20
25
Concentration of TRACP-5b (U/L)
R² = 0.9968
R² = 0.9908